DOI: 10.13009/EUCASS2017-79

Visualization coupled with Phase Doppler Interferometry for investigation of cryogenic LOX/nitrogen and LOX/helium sprays

N. Fdida, Y. Mauriot*, L. Vingert*, A. Ristori * and M. Théron***
**Onera – The french Aerospace Lab, F-91761 Palaiseau, France*
*** CNES – Launcher Directorate, 52 Rue Jacques Hillairet, 75012 Paris*

Abstract
There is a need of experimental data in injection conditions representative of rocket engines to validate or initiate droplet formation models used in numerical simulations. A new cryogenic vessel was built upon the Mascotte test bench to study the atomization of a single oxygen liquid jet, under non-reactive conditions, with simultaneous optical diagnostics. A Phase Doppler Interferometer is used to measure the size and velocity of droplets produced by atomization of a liquid oxygen jet by a co-flowing gas. Among the tested injection conditions, the influence of the gas density on the spray is investigated here with two atomizing gases: helium or nitrogen.

1. Introduction

In liquid propellant rocket engine combustion, physical processes such as atomization, mixing or vaporization of propellants are complex and can interact with one another. Thermo-acoustic instabilities can develop during the transient operating states of the engine and lead to its deterioration. Atomization is a dominant process that drives the behaviour of such a cryogenic flame, particularly when the propellants are injected in subcritical conditions, investigated by several research teams ([1], [2] and [3]). Atomization therefore needs to be studied in order to better predict the occurrence of these high frequency instabilities. ONERA and CNES have a common interest to improve the knowledge on cryogenic atomization in liquid propellant rocket engines, in order to build reliable physical models and validation databases for CFD codes. The validation and initialization of recent numerical simulations ([4] and [5]) requires experimental data in the atomization zone, situated close to the injector inner LOX post. In this two-phase flow, combustion makes measurements and simulations very tough, so atomization is studied without the presence of the flame in order to predict the spray formation more efficiently.

A new experimental configuration, presented by Mauriot et al., 2016 [6], is built upon the Mascotte test bench. It is dedicated to study the atomization of the liquid oxygen jet (LOX) with simultaneous optical diagnostics. This cryogenic Flow Visualization Box (BVF) is fully instrumented with pressure and temperature transducers and can be pressurized in a wide range of chamber pressures, flow rates and fluid temperatures under conditions which are inert but nonetheless representative of industrial conditions concerning the fluids injection.

The BVF was designed to operate simultaneously high-speed diagnostics such as interferometry Phase Doppler and high-speed visualization. Coupling those complementary diagnostics is very useful to understand the dynamics of atomization considered as a multiscale phenomenon. Thus, imaging provides large as well as close field of views, according to the optical setup, to visualize either the overall spray or focus on the droplet sizes or velocities [7]. In these operating conditions, the use of the PDI is more adapted than imaging to measure droplet sizes and velocities. Consequently, the field of view is large to visualize the PDI measurement volume located close to the injector post, in the primary atomization zone, where droplets are mainly created by the liquid/gas shear interface.

DOI: 10.13009/EUCASS2017-79

2. Materials and methods

2.1. The Mascotte test bench

2.1.1. BVF Flow Visualization test vessel

The Mascotte test facility was developed at ONERA in order to investigate physical phenomena involved in the combustion of cryogenic propellants [8], such as atomization, mixing, vaporization, combustion instabilities... Among these, atomization remains a key issue, especially in subcritical pressure conditions. To decouple the atomization from combustion in the atomization process, a new cryogenic test cell was built to study a liquid oxygen jet atomized with cold gaseous N_2 or He. The cryogenic test vessel, called BVF, is shown on figure 1; it was designed with large inner dimensions in order to limit spray interactions with walls and windows. Moreover, the internal part of the windows is protected from droplets impacts by a gaseous film on the windows. An external heating device protects the windows from icing, as seen on figure 1. The BVF is fully instrumented in pressure and temperature transducers. It is compatible with laser measurements close to the injector exit, with a pressurization up to 30 bar and is able to reach fiber-type injection conditions, i.e. high Weber number ($>10^3$) and Reynolds number ($>10^4$) and a momentum flux ratio J > 1, representative of a liquid rocket engine injection device. The four windows have the same dimensions and are located at the same height; three of them are placed at 90° of each other, the fourth one is placed at an angle optimized for Phase Doppler droplet sizing (145° between emitter and receiver). The total duration of a typical test sequence is about 130 seconds where the stationary phase of the flow is about 40 seconds, necessary for the PDI to measure a sufficient number of droplets.

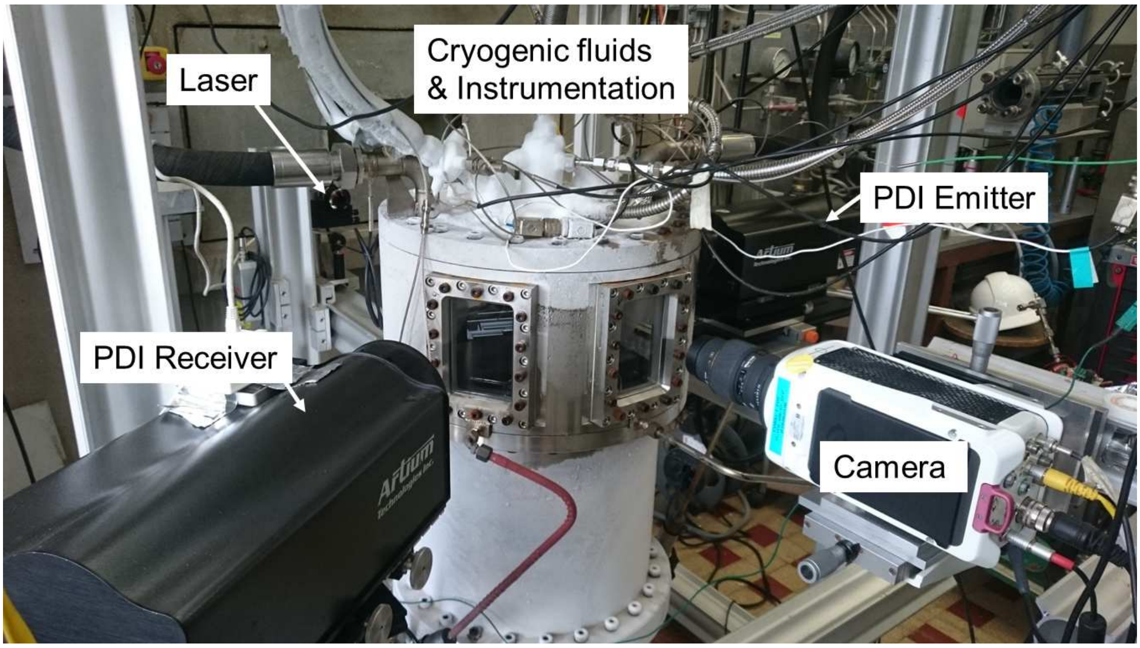

Figure 1: Optical setup around the cryogenic test chamber

2.1.2. Injection configuration

The cryogenic fluid lines are regulated in temperature from the tank to the injection head of the vessel. The atomizing gas injection temperature is maintained as close as possible to the LOX temperature (difference less than 10 K). The coaxial injector, characterized by its internal diameter D_L, is visible inside the field of view in order to see the LOX jet from the exit of the injector to a distance of it equal to several times its diameter.

Lasheras and Hopfinger [11] proposed a classification of breakup regimes for a coaxial jet as a function of three parameters: the gaseous Weber number $We_G = \rho_g U_g^2 D_L/\sigma$ (based on the LOX post diameter D_L, the gas density ρ_g, the gas velocity U_g and the surface tension σ), the Reynolds number $Re_L = U_L D_L/\nu_L$ (based on the LOX post diameter D_L , the liquid jet velocity U_L and the viscosity ν_L) and the gas-to-liquid momentum flux ratio $J= \rho_g U_g^2$ $\rho_L U_L^2$. We consider that typical injection conditions of a liquid rocket engine are characterized by $We_G > 10^3$,

DOI: 10.13009/EUCASS2017-79

$Re_L > 10^4$ and $J > 1$. This breakup regime is known as the fiber type atomization, and by fixing the liquid jet velocity, the test plan explores the influence of the gas velocity, the injector geometry or the atomizing gas density, which are the main parameters driving such an atomization process [11]. The operating points shown on the (We_G, Re_L) diagram on figure 2 are distributed along a fixed Reynolds line, with variations of the Weber number as well as the J number. On this diagram, symbols represent the operating conditions investigated during two experimental campaigns performed in 2015 and 2016. The generic operating conditions are called xN or xH, respectively for Nitrogen and Helium as atomizing gas, where "x" is an arbitrary number. 8N and 8H were chosen so as to have values of the J number as close as possible. Lines of constant J appear as straight lines in logarithmic coordinates for constant values of D_L *and* V_L, according to the relation $Re_L = (We_G/J)^{1/2}(D_L\,\sigma/\rho_L V_L^2)$, the dashed line corresponding to J=1 in the water/air experiment [11] and the solid ones to a liquid oxygen/inert gas mixing. In our study, the momentum flux is varying in the range $1< J < 12$ and the dimensionless number domain is within the fiber-type regime, with $2000 < We_G < 12000$ and a fixed Reynolds number $Re_L \approx 65000$. The numbers are calculated during the stationary phase of the flow with the transducers equipping the BVF. Nine typical instantaneous images are also shown on this diagram. The We_G varies from 2000 to 11000, under the effect of the gas injection velocity U_G and the gas density ρ_G.

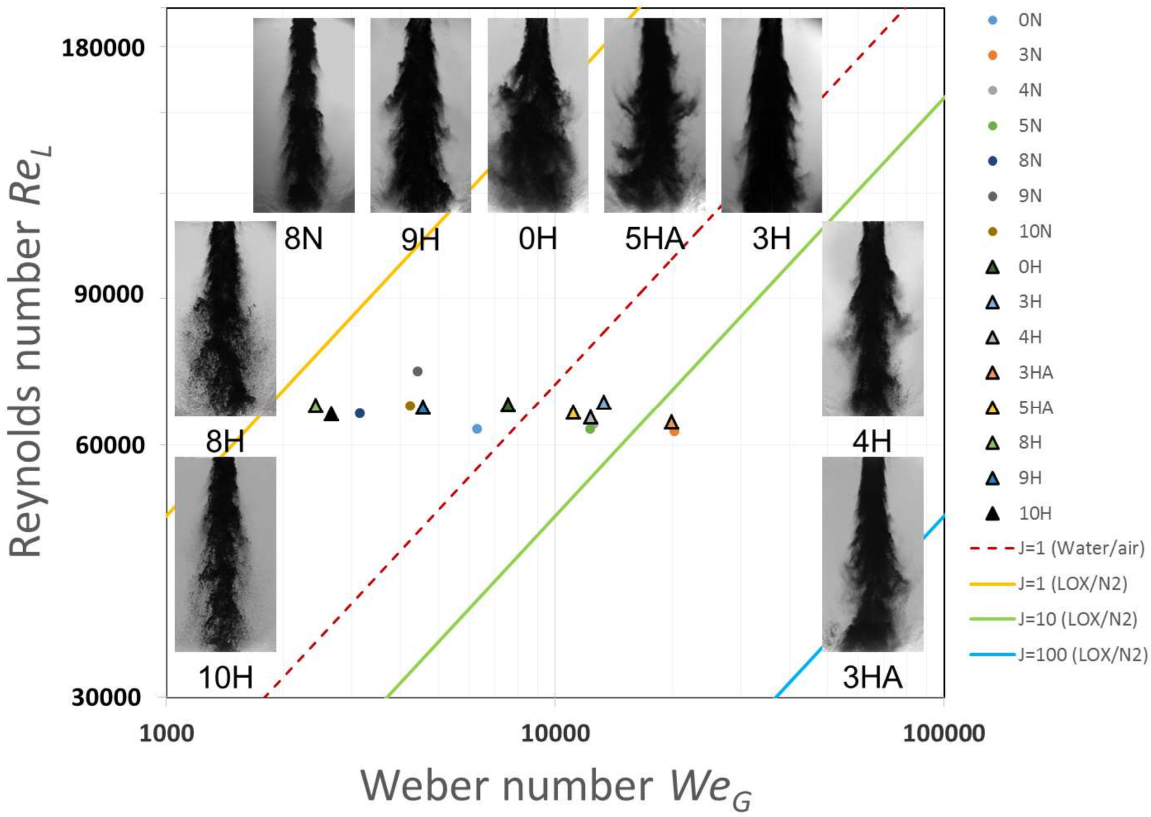

Figure 2: Injection parameters of the fiber-type regime in (We_G, Re_L) diagram

The test plan was built to explore the LOX jet atomization in a fiber-type break-up regime, which is characterized by the creation of very thin and short liquid fibers created as soon as the continuous liquid jet exits from the nozzle. These fibers are rapidly peeled off the jet, stretched by the differential velocity between the liquid jet and the outer gas stream, from which depends the Weber number. Due to this stretching, the liquid jet is highly modified and disintegrates into liquid filaments which, in turn, are broken, creating droplets [12]. The characteristic break-up time is very short, which means a rapid atomization of the majority of the liquid. The droplets are produced in very small sizes, several orders of magnitude smaller than the diameter of injection. An illustration of such a process is shown on figure 3 where a set of successive images recorded at 16 kHz evidences a longitudinal primary instability developing at the injector exit, creating fibers which collapse into droplets.

DOI: 10.13009/EUCASS2017-79

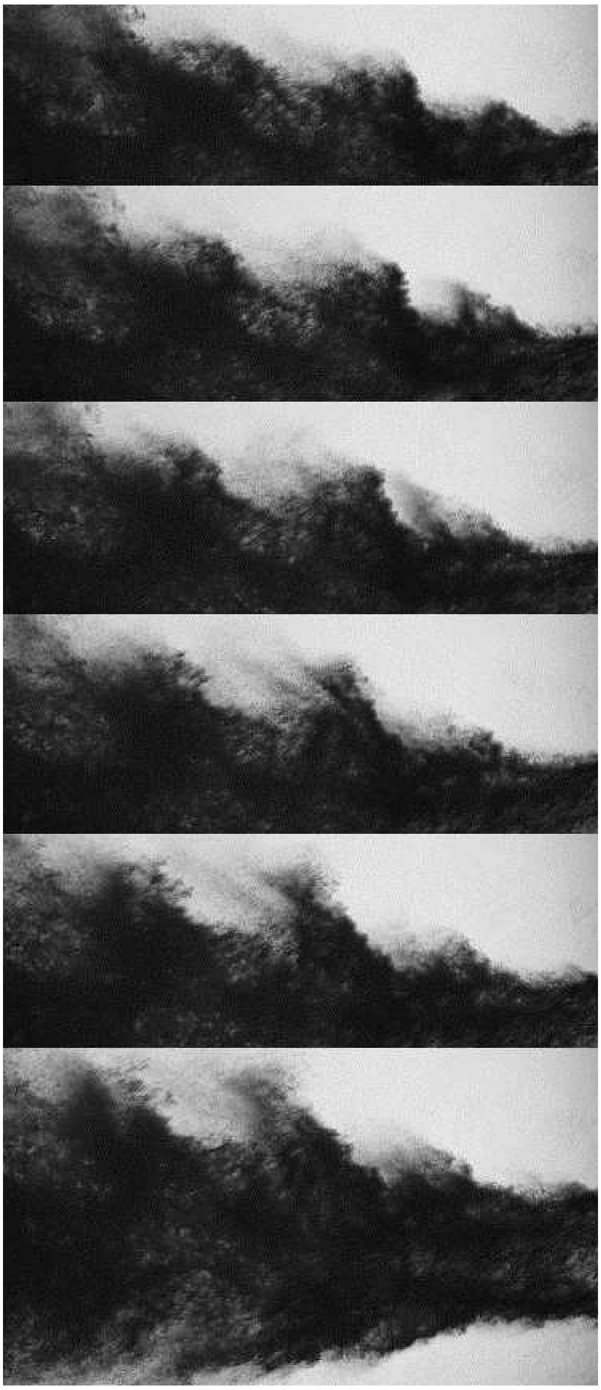

Figure 3: Illustration of the primary atomization with instantaneous successive images recorded at 16 kHz for 0H case.

DOI: 10.13009/EUCASS2017-79

2.2. Optical Setup

A Phase Doppler Interferometer (PDI) is used simultaneously with a high-speed camera thanks to the particular four windows arrangement on the BVF.

2.2.1. High-speed shadowgraphy

A high-speed camera shadowgraphy setup is used to visualize where the droplets are present in the spray in order to detect the region of interest for the spray exploration with the PDI. The spray is enlightened in a backlight configuration by a laser diode CAVILUX Smart 400W which emits a red incoherent light pulse at 640 ±10 nm. This source is very compact and stable in space and time, enlightening the LOX jet through an optical fiber. The pulse duration can be set in a large range of time periods, from 0.02 µs to 10 µs, with 0.01 µs steps. In our application where droplets velocities are very fast, we fixed the pulse duration to 0.04 µs to freeze the droplets on the images and avoid any blurring effect. The repetition rate can be set from 25 Hz to 10 kHz continuously and can be increased to 50 kHz during limited periods. A Fourier lens of 50 mm focal length is placed at the fiber exit, as well as a diffuser to create a large illumination area to see the spray in a large field of view, as shown on figure 2.
Images of the spray were recorded with a Phantom v711 high-speed camera from Vision Research. This camera is composed of a 12-bit CMOS sensor of 1280 x 800 square pixels and of 20 µm side length. The resolution of the sensor is directly related to the frequency rate. The sensor resolution was set at 800 x 400 px² at 25 kHz or 1024 x 512 px² at 16 kHz. The camera is equipped with Sigma lens of 105 mm focal length and a narrow band pass filter centred on the red illumination wavelength of the light source. Hence green and blue beams coming from PDI are not recorded by the camera.

2.2.2. Phase Doppler Interferometer

The Phase Doppler Interferometer (PDI), from ARTIUM Inc, is a particle counter which was used to measure the oxygen droplet size and velocity distribution in the LOX spray, under steady operating conditions. A solid state laser system delivers green (λ_g = 532 nm) and blue beams (λ_b = 491.5 nm). The focal length of the emitter lenses was set to 350 mm and the one of the receiver was set to 500 mm, constituting a setup adapted for such a dense spray. The off-axis angle of the receiver was set to 35° as recommended by the manufacturer, for the expected droplet size range (the basics of this instrument are presented in [13]). The PDI was set with a 50 µm slit aperture on the receiver to collect a thin part of the light coming from the measurement volume. Indeed, in order to avoid multiple droplet signals we chose a short focal length at emission together with a small aperture on the receiver, which resulted in a short measurement volume [14].

The estimated refractive index n of the LOX droplets indicated to the PDI is fixed to n=1.21, according to the work of Johns and Wilheim [15], in order to ensure an uncertainty of ±2% on the diameter size measurement in the temperature range from injection to boiling temperature in the test chamber thermodynamic conditions. Based upon the presented optical setup, the PDI could measure droplet diameters within the range 1 µm < D < 108 µm. The PDI provides two components of the droplet velocity (horizontal Vx and vertical velocity Vz, respectively through blue and green channel). The largest velocity range in our acquisitions was -20 m/s < Vx < 20 m/s and -75 m/s < Vz < 200 m/s for horizontal and vertical velocity, respectively. The directions of the measured velocities are defined on figure 4.

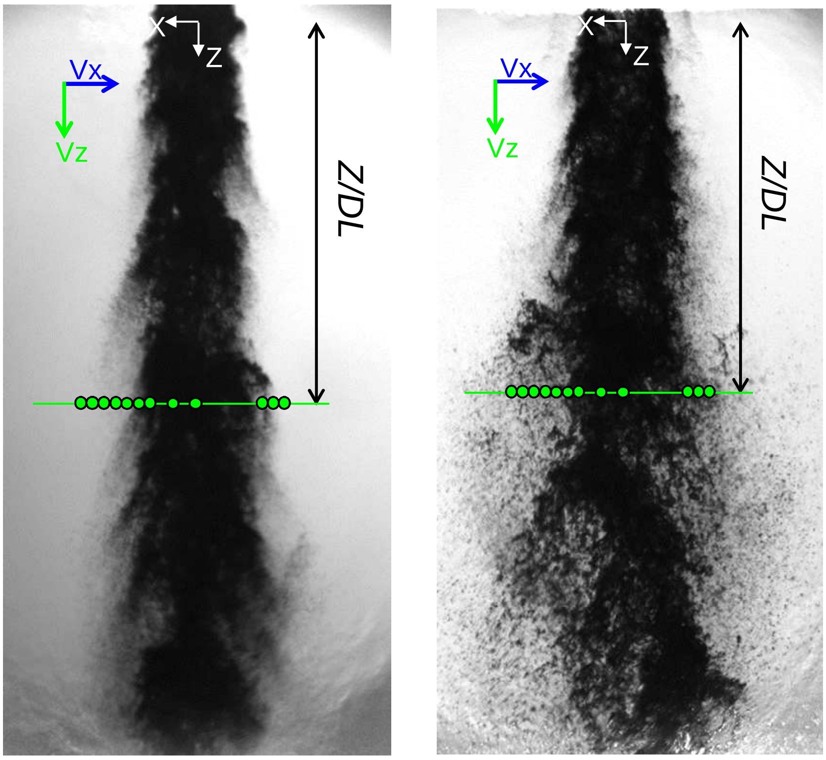

a) LOX/N2 injection, 8N ter *b) LOX/He injection, 8H*

Figure 4: Location of PDI measurements from the injector inner post; Vx, Vy are velocities measured by PDI

2.2.3. Measurement locations

Obviously, PDI measurements can only be performed where droplets are present. Images recorded by the high-speed camera are helpful to identify the two-phase flow density targeted by PDI. An example of instantaneous shadowgraphs is presented in the background of figure 4, superimposed with the PDI measurement locations, illustrated by green dots. PDI measurements are performed in a vertical plane Y=0, crossed by the injection axis. In this plane, at a vertical position Z/D_L, transverse profiles were made along the X axis, spaced by X/D_L, straight under the injector gas gap, in the two-phase flow area. Diameter and velocity measurement were made at a close distance from the nozzle exit Z/D_L, with Z/D_L <5. The coordinates of the PDI measurement volume are known, relatively to the injector reference system, thanks to a graduated object that is mechanically fixed to the injector. It ensures an uncertainty in position of ±0.5 mm and ±1 mm, respectively on X and Y axis, corresponding to the PDI optical axis. For each operating condition, a set of 5 to 10 PDI measurement locations is obtained depending if droplets are actually collected at each location.

Droplets are collected during 35 s in the stationary phase of the flow, the number of droplets obtained in the sample varies from few one to several thousands, depending on the PDI validation rate. The validation rate is the percentage of droplets that are accepted by the instrument as being spherical drops. It varies from a few percent to 65%, depending on the PDI location in the spray. The lowest validation rates are obtained close to, or inside the liquid jet ($|X/D_L|<0.5$). The highest validation rate reaches 64% for the measurement point located at the center of the line of points (($|X/D_L|\sim1$), with 124000 droplets detected in 25 s. To achieve a reasonably accurate estimate of the mean diameter D_{10} of the droplet sample, samples of at least 1500 measurements are necessary (which allows a +/-10% accuracy on D_{10} [10]).

3. Results and Discussion

3.1. High-speed visualizations

Time-averaged (top) and RMS (bottom) images are shown on figure 5 for four operating points with LOX/N_2 and LOX/He, increasing J and Weber number. Considering 8H and 8N cases (with close values of J), one can notice that the spray plume is thinner when N_2 is the atomizing gas. A previous experimental study [16] evidenced an effect of axial and radial reduction of the LOX core with a gas density increase, due to an intensification of the primary

DOI: 10.13009/EUCASS2017-79

breakup. According to this hypothesis, nitrogen being a denser gas than helium should lead to an intensification of the atomization process, which is the observed tendency. The effect of the produced liquid elements can be seen as straight lines on the RMS images at left.
Increasing the Weber number tends to enlarge the spray plume on time averaged images from 8H to 0H and 3HA case (the injector geometry is fixed and the Helium gas velocity is increasing). Moreover, from left to right on figure 5, the RMS images show that as the Weber number increases, the high fluctuations contour area becomes finer. In this area which is distributed close to the LOX jet for 3HA, a large proportion of tiny droplets is produced, creating sometimes a wall for light to be collected by PDI or imaging. For the 8H case, the liquid element production is mainly distributed on the edge of the spray.

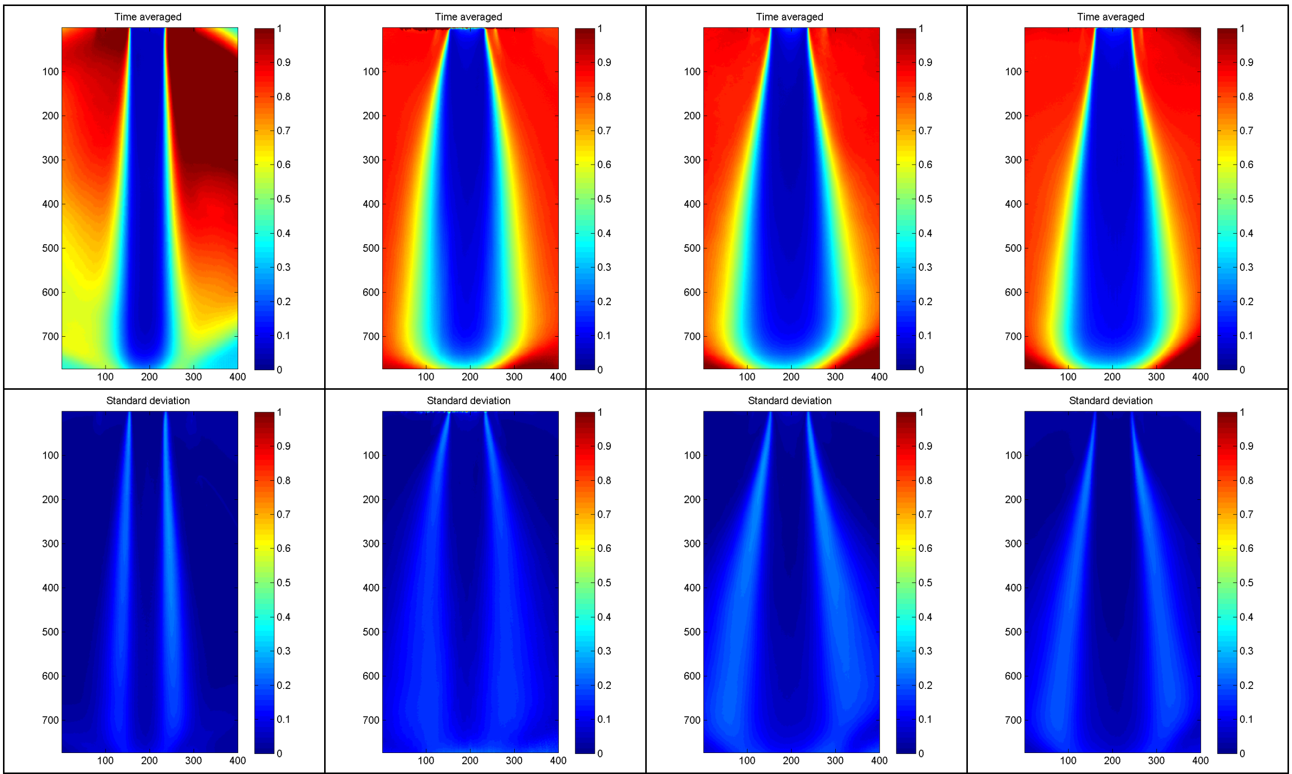

8N (J=1.9, We_G=2.10^3)	8H (J=1.4, We_G=3.10^3)	0H (J=4.3, We_G=7.10^3)	3HA (J=11.7, We_G=2.10^4)

Figure 5: Time averaged and RMS images for four operating conditions

3.2. Droplet velocities

The effect of the atomizing gas N_2 or He can be studied with PDI measurements on figure 6: mean droplet axial velocity is plotted versus the radial position of the measurement volume for three operating points: 8N, 8H and 4H. The size of each disc representing a PDI point is directly proportional to the mean droplet diameter D_{10}. We notice that for a defined operating point the more rapid is the axial velocity, the smaller is the mean drop size indicating that the droplet size is driven by the We_G, as proposed by [17]. The velocity radial profiles are not symmetric with respect to the injection axis, showing that the perpendicularity between the orientation of the injector axis and the PDI velocity orientation is barely satisfactory. The increase of the axial velocity with radial distance from the centreline was evidenced by Pal et al. [3] on water/N2 shear coaxial injectors and they also noticed that the velocity reaches a maximum at radial distance $X/D_L > 2$, and then decreases for greater radial distance. Due to a lack of droplets for distance $X/D_L > 1.5$, we did not obtain PDI results so far from the injection axis. This lack of droplets could be explained by the measurement volume location which is closer to the injector inner post ($Z/D_L<5$) whereas in other studies, the PDI axial location is usually further downstream at $Z/D_L \geq 10$ for [3] or [16].

DOI: 10.13009/EUCASS2017-79

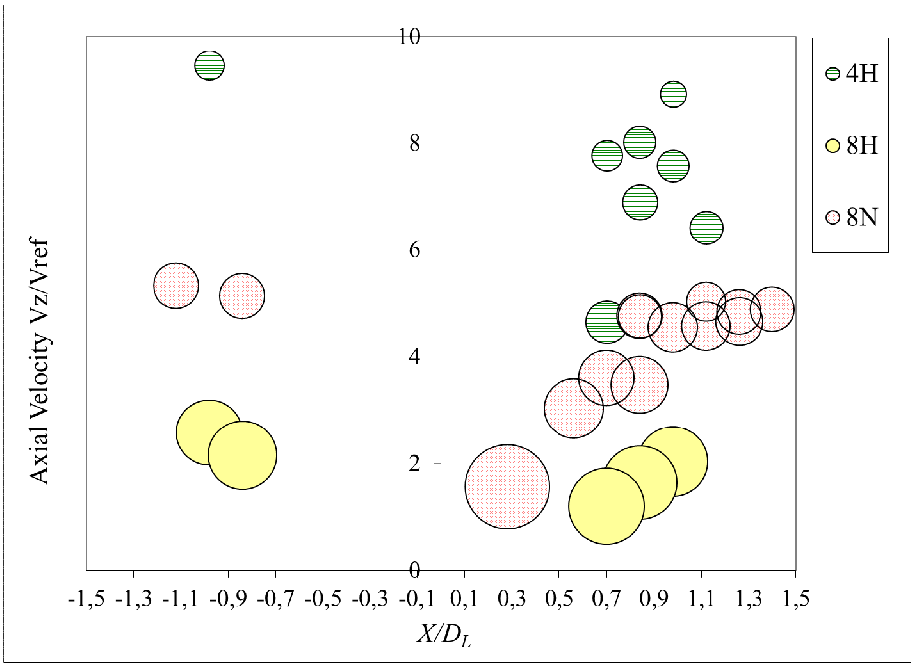

Figure 6: Overview of the radial velocity profiles measured by PDI in different test cases 8N, 8H and 4H

3.1. Drop-size measurements

From 8N case data shown on figure 6, the radial evolution of the mean droplet size D_{10} slightly decreases radially until X/D_L=1 and then, as the distance from the injector axis increases the trend is less clear. The decrease of mean diameter has also been observed by Pal et al.[3] on a spray produced by a water/N2 shear coaxial injector and phase Doppler measurements. They also noticed an improvement of primary atomization with the increase of the momentum flux ratio J, inducing a decrease of the mean drop size.

The radial evolution of the drop size is also presented on figure 7, by the pdf (probability density functions) of the operating point 8N. The above mentioned trend is clearer with such a diagram: the mean drop size decreases radially as the pdf is translated towards the small sizes. The smallest droplets are encountered at the furthest position from the LOX jet axis, on the edge of the spray for X/D_L=1.4. For this position on the edge of the spray, the PDI data rate (droplets collected by second) is relatively low because the droplet density (number by volume) is small, it takes time to acquire data even with a good PDI validation rate (> 60%). Such a high validation rate probably indicates that most of droplets are spherical, for this position in the spray. As the PDI measurement location comes closer to the LOX jet, the PDI counts more particles by second but the validation rate is lower and usually a validation rate of about 20% is obtained around $X/D_L=1$. The biggest liquid elements of the drop size stay close to the center of the liquid jet, due to their inertia, as their radial velocity V_x, obtained by PDI diameter/velocity correlation (not shown here), is low. Droplets are smaller on the edge of the spray due to the effect of aerodynamic forces as well as vaporization, reducing the droplet size. On the other side, as the PDI measurement location comes closer to the injection axis, the overall shape of the pdf is translated towards bigger diameters, until X/D_L =0.56.

DOI: 10.13009/EUCASS2017-79

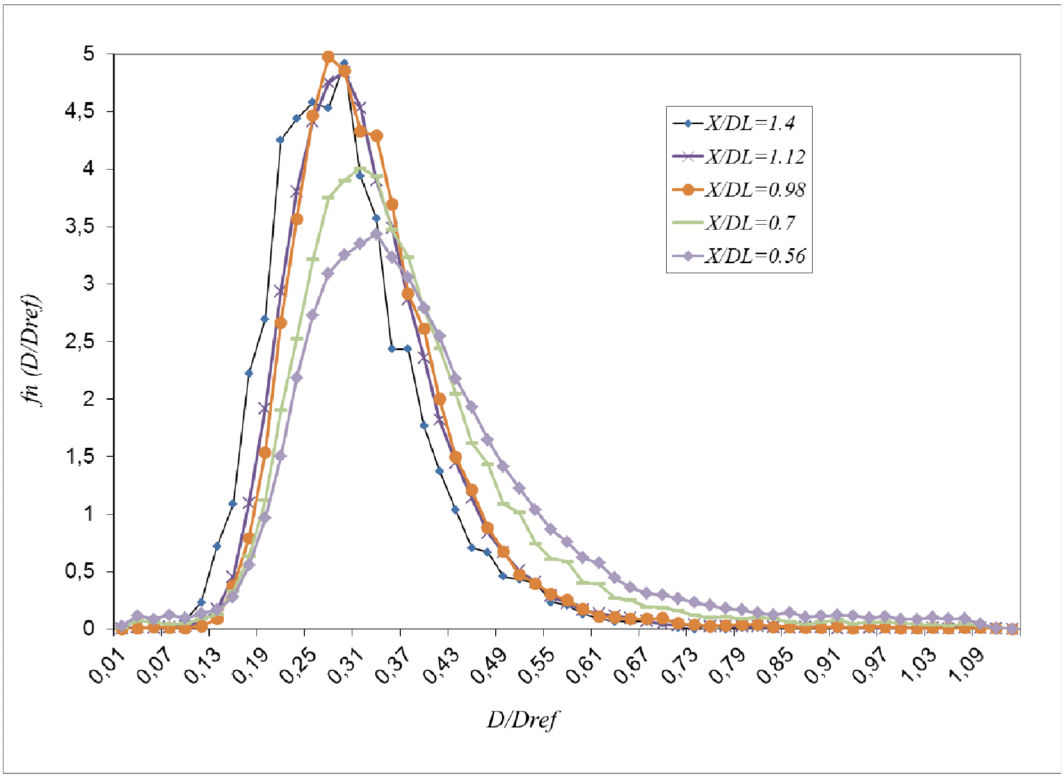

Figure 7: Radial evolution of LOX droplet sizes for 8N case (X/D_L=1, Z/D_L=4.5)

4. Conclusion

Understanding the physics of the atomization for a specific injector is important for building theories on the subsequent dynamics of vaporization, mixing and combustion. Those theories can only be validated by experimental data that detail the droplet-size and velocity distributions under various operating conditions, reacting or inert. There is a lack of experimental data in the liquid rocket engine literature because of the harsh environment for optical diagnostics in liquid propellant rocket engines, the safety aspects to consider when working with liquid oxygen and the expensive nature of the experiments. With the support of CNES, this experimental campaign led to drop-size and velocity measurements in various operating conditions in order to describe the spray produced by a shear coaxial injector in non-reactive conditions, representative of a single element of a liquid rocket engine. The Reynolds and Weber number ranges are closer to the conditions of actual rocket engines than in our previous experiments investigating the primary atomization zone. This experimental test campaign in inert conditions was very fruitful of data in terms of injection conditions and greatly increased the database of the Mascotte experimental non reacting injection cases. This database will help to build atomization models for predicting initial drop size distribution that are integrated in more complex CFD codes. Indeed, the locations of the PDI measurement points are close to the injector at a distance that could be used to initiate the primary breakup processes.
The perspective of this work is to fit the experimental distributions on mathematical models existing in the literature, the log-normal and the gamma law for example, to link the pdf shape to the physical parameters driving the atomization process. We are also focused on the reacting cases and building an experiment to measure the droplet size and velocity in an experimental fire test case, within a LOX/H2 jet flame, in fiber type injection conditions, to address the influence of the flame on the drop size produced by a shear coaxial injector.

Acknowledgments

A part of this work has been co-funded by the Centre National d'Etudes Spatiales (CNES) and by ONERA, in the framework of a common interest program dedicated to the study of high frequency instabilities.
The authors thank Mr Carru, Vannier and Paux for their assistance in conducting the experiments.

DOI: 10.13009/EUCASS2017-79

References

[1] Candel S., M. Juniper, P. Scouflaire, C. Rolon, W. Clauss, D. Klimenko, M. Oschwald, and L. Vingert. 2003. Investigations of subcritical and transcritical cryogenic combustion using imaging and laser techniques. In: *5th International Symposium on Space Propulsion*, Chattanooga, USA. 27–30.

[2] Mayer W., and H. Tamura. 1996. Propellant injection in a liquid oxygen/gaseous hydrogen rocket engine. Journal of Propulsion and Power. 12:1137-1147.

[3] Pal S., M. D. Moser, H. M. Ryan, M. J. Foust, & R. J. Santoro. 1993. Flowfield characteristics in a liquid propellant rocket. In: *AIAA/SAE/ASME/ASEE 29th Joint Propulsion Conference and Exhibit, Monterrey*, USA. 27–30.

[4] Murrone A., N. Fdida, C. Le Touze, L. Vingert. 2014. Atomization of cryogenic rocket engines coaxial injectors. Modeling aspects and experimental investigations. In: *Space Propulsion 2014*, Köln, Germany.

[5] Vaudor G. 2015. Atomisation assistée par un cisaillement de l'écoulement gazeux. Développement et validation. PhD Thesis. University of Rouen, France.

[6] Mauriot Y., N. Fdida, L. Vingert, S. Godel, A. Ristori, M. Théron. 2016. Characterizing coaxial primary atomization without combustion on the MASCOTTE test bench. In: *Thermoacoustic Instabilities in Gas Turbines and Rocket Engines: Industry meets Academia*, Munich, Germany.

[7] Fdida N., L. Vingert, A. Ristori, Y. Le Sant. 2016. Drop size and velocity measurements in a cryogenic jet flame of a rocket type combustor using high-speed imaging. *Atomization and Sprays*, vol. 26, Issue 5, p. 411-438.

[8] Habiballah M., M. Orain, F. Grisch, L. Vingert, P. Gicquel. 2006. Experimental studies of high-pressure cryogenic flames on the Mascotte facility. *Combustion Science and Technology*, vol.178, p.101-128.

[9] Marmottant P. and E. Villermaux. 2004. On spray formation. *J. Fluid Mech*. Vol. 498, pp. 73–111.

[10] Lefebvre, A.H. 1989. Atomization and Sprays. Hemisphere Publishing Corp.

[11] Lasheras J.C. and E. J. Hopfinger. 2000. Liquid Jet Instability and Atomization in a Coaxial Gas Stream. *Annual review of Fluid Mechanics.* Vol. 32, pp.275-308.

[12] Vingert L., P. Gicquel, D. Lourme, L. Menoret. 1995. Coaxial Injector Atomization. Liquid Rocket Engine Combustion Instability. *Progress in Astronautics and Aeronautics*. Vol. 169, pp. 145-189.

[13] Strakey P., D. G. Talley, S. V. Sankar and W. D. Bachalo. 2000. Phase-doppler interferometry with probe-to-droplet size ratios less than unity. I. Trajectory errors. *Applied Optics.* Vol. 39(22), pp.3875–86.

[14] Bachalo W. D., G. A. Payne, C. M. Sipperley and K.M. Ibrahim, Advances in the Phase Doppler Method for Dense Spray Measurements, In: *Proceedings of ICLASS 2015*, Tainan, Taïwan (2015).

[15] Johns H.E. and J.O. Wilheim. 1937. The refractive indices of liquid oxygen, nitrogen and hydrogen, *Canadian Journal of Research*, Vol. 15, Sec. A, n°7.

[16] Porcheron E., J.-L. Carreau, D. Le Visage et F. Roger. 2002. Effect of Injection Gas Density on Coaxial Liquid Jet Atomization. *Atomization & Sprays*, Vol. 12, No. 1-3, pp.209-227.

[17] Ben Rayana F., A. Cartellier and E. Hopfinger. 2006. Assisted atomization of a liquid layer: investigation of the parameters affecting the mean drop size prediction. In: *proceedings of ICLASS-2006*, Kyoto, Japan.

[18] W.A. Sowa. 1992. Interpretating Mean Drop Diameters Using Distribution Moments, Atomization & Sprays, Vol.2, pp.1-15.